



Development of an electrochemical sensor based on aniline, N-phenylglycine, graphene oxide and p-tertbutyl-calix-[4]-arene for trace detection of uranium ion from water

Kusumita Dutta^{1,2} · Siddhartha Panda^{1,2}

Received: 13 March 2024 / Accepted: 29 June 2024
© The Author(s), under exclusive licence to Springer Nature B.V. 2024

Abstract

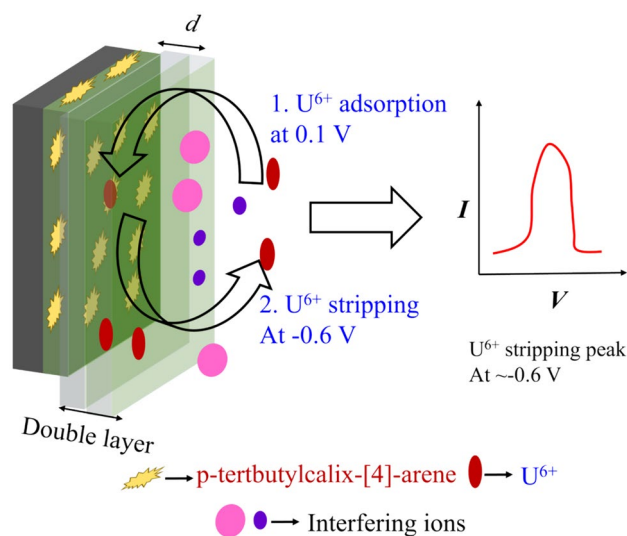
Selectivity and sensitivity are prime parameters while constructing a sensor. Due to rapid development of nuclear industry, the uranium exploitation has created pollution problems in nature. The naturally occurring uranyl ion U^{6+} is carcinogenic and toxic in nature posing a significant threat to human health. Therefore, it is necessary to construct a U^{6+} sensor which is selective as well as sensitive to U^{6+} and can be useful for measuring U^{6+} in drinking water. In this work, a novel composite was electrochemically synthesized from aniline, N-phenylglycine, graphene oxide and p-tertbutylcalix[4]arene. Square wave voltammetry experiments to detect U^{6+} were performed and limit of detection (LOD) of 900 ppt (~ 2.273 nM) was obtained. Interference study was carried out with a large number of test ions (Ru^{3+} , Cs^+ , As^{5+} , Cr^{6+} , Cu^{2+} , Na^+ , Mg^{2+} , Al^{3+} , K^+ , Sr^{2+} , Mn^{2+} , Fe^{3+} , Fe^{2+} , Zn^{2+}) by both peak reduction (PR) technique and barrier width (BW) technique. The conventional technique for interference analysis is PR technique, requires series of experiment to predict interference. BW technique, requiring handful number of experiments, is the one which, for aqueous ion sensor, was introduced for the first time to investigate interference towards the target analyte (Cd^{2+}), in our previous works. In this work, the results obtained from PR technique showed that only Ru^{3+} , Cs^+ , Cr^{6+} and Cu^{2+} interfere U^{6+} . BW technique results support the results obtained by PR technique. The novel sensing material synthesized in this work has been used for the first time for uranyl ion detection with less interference. It has the advantage of easy synthesis procedure requiring no surface modification, leading to a LOD of 4 ppb for U^{6+} in presence of interfering ions which is far below the permissible limit for U^{6+} in drinking water.

✉ Kusumita Dutta
kusumitasword@gmail.com

¹ Department of Chemical Engineering, Indian Institute of Technology Kanpur, Kanpur 208016, India

² National Centre for Flexible Electronics, Indian Institute of Technology Kanpur, Kanpur 208016, India

Graphical abstract



Keywords Square wave voltammetry · Adsorption · Sensitivity · Barrier width · Metal ion detection

1 Introduction

The toxicity of uranium is widely accepted problem to be dealt with [1–4]. Generally, uranium exposure to human is from hazardous waste from nuclear plant, sewage or laboratory wastewater from nuclear plant, industrial waste as well as rock soil erosion [5–9]. Uranium is present in nature as ^{238}U , ^{235}U and ^{234}U [10–12]. Among them, the analyte of interest in this work was ^{238}U which is present in nature in aqueous ion form as U^{6+} . The toxicity of uranium leads to several diseases including cancer [13–15], nephrotoxicity, genotoxicity, developmental defects [13, 16]. The maximum permissible limit for uranium in drinking water is 30 $\mu\text{g/L}$ (~ 30 ppb) [17]. Recent reports verify that there is significant uranium contamination in ground water in various places of Indian subcontinent region [18–25]. It has been reported that the uranium contaminant in ground water has been exceeded the maximum permissible limit in several places in Punjab [26]. Therefore, it is highly necessary to fabricate a low-cost uranyl ion sensor. The conventional detection techniques available for uranyl ion are atomic absorption spectroscopy [27], inductively coupled plasma mass spectroscopy [28, 29], laser induced fluorescence [30], X-ray fluorescence spectrometry [31], laser Raman spectrometry [32], optical emission spectrometry [33, 34]. Although these provide accurate results, the main problems associated with these techniques are high operating and maintenance cost [33], some having lower sensitivity [35] and most importantly, they lack online monitoring capability [33]. Moreover, in few cases, interference is also an issue. Therefore, a low-cost

suitable online monitoring system is necessary to detect uranyl ion qualitatively and quantitatively with high selectivity. Electrochemical detection techniques overcome all these issues [4, 9, 36–41]. One such electrochemical technique is square wave voltammetry (SWV).

Selectivity, sensitivity and low limit of detection (LOD) are the prime parameters to construct an electrochemical sensor. Polyaniline, being a conducting polymer, has been used widely to detect heavy metal ions [42–45]. In our earlier works [46–48] polyaniline-based electrode was used for detection of Cd^{2+} ions by SWV. A novel composite from aniline, N-phenylglycine and graphene oxide (GO) was synthesized to detect Cd^{2+} with lesser interference from several ions. Polyaniline-based material has a variety of applications but due to its incompatibility, infusibility and modest environmental stability due to its rigid chain structure, makes it un-processable. Therefore, incorporation of electron withdrawing group such as $-\text{COOH}$ can improve its processability. N-phenylglycine has one electron withdrawing group $-\text{COOH}$ and has similar structure to that of aniline. Incorporation of N-phenylglycine improves the reactivity by providing additional active sites [49]. It was observed that the reactivity, and electrochemical surface area of the composite synthesized from aniline, N-phenylglycine and GO was higher than those from the composite synthesized from aniline and GO, as shown in our earlier work [48]. For interference analysis, conventional peak reduction (PR) technique was used and a novel barrier width (BW) technique employing electrochemical impedance spectroscopy (EIS) and cyclic voltammetry (CV), was introduced for the first

time in case of aqueous ion sensor. PR technique requires a series of experiments to predict the interference while BW technique overcomes this issue by requiring a handful number of experiments. Subsequently this BW technique was benchmarked with PR technique for interference analysis. In this work, another composite based on aniline, N-phenylglycine and GO and a ligand was used to detect U^{6+} and both the PR and BW techniques were used to study the interference of a series of test ions towards U^{6+} ions. To enhance the sensitivity and selectivity a number of suitable ligands or components are reported in literature used as complexing agents for U^{6+} . These are L-DOPA [50], 8-hydroxyquinoline [51], chloranilic acid [52], arsenazo (II) [53], cephradine [54], TriBAP, TetraBAP [55], cupeferron [56–58], dipicolinic acid [59], PAA [60]; or as complexing agent at the electrode surface, e.g. 4sulfonic-calix[6]arene [61], 4-carboxyphenyl [62], carbamoylphosphonic acid [63], DNAzyme [64], phosphorothioated oligonucleotides [65]. p-tertbutyl calix[4]arene is one such ligand which can be used to detect U^{6+} . There are several reports where composite made from polyaniline or GO and p-tertbutyl calix-[4]-arene have been used for water purification or in catalysis [66–69]. Guo et al., have synthesized chemically a composite of polyaniline and p-tertbutylcalix-[4]-arene as adsorbent for water purification [66]. Similarly Mohammadi et al., have synthesized an adsorbent from Polyurathane foam and p-tert-butyl thiacalix [4] arene, by chemical synthesis route, used for water purification [67]. Again Mohammadi et al., have used a composite synthesized by chemical means from Alginate, GO, p-tert-butyl calix[4]arene, sodium p-sulfonatocalix[4]arene and used it for water purification [68]. Zhang et al., have chemically synthesized a composite from GO, p-tertbutyl calix-[6]-arene and used as adsorbent [69]. Gutsche et al., have used P-tert butyl calix-[6]-arene—GO composite, synthesized by chemical route, and have used for catalysis [70]. Hyder et al., synthesized para-dimethylamine calix[4]arene modified self-assembled GO and used as adsorbent [71]. C-undecylcalix[4]resorcinarene and reduced GO based composite was synthesized by Wu et al., for detection of tryptophan [72]. There is no report till date where a composite from aniline, N-phenylglycine, GO and p-tertbutyl calix[4] arene was used to detect U^{6+} and here lies the novelty of this work.

In this work a novel composite from aniline, N-phenylglycine, GO and p-tertbutylcalix[4]arene, was synthesized for the first time by electrochemical route and used to detect U^{6+} by SWV. The surface morphology of the sensing film was achieved by FESEM and HRTEM and the material characterization was carried out by FTIR. Sensitivity of the system was evaluated, and adsorption isotherm was constructed. Interference of various test ions (Ru^{3+} , Cs^+ , As^{5+} , Cr^{6+} , Cu^{2+} , Na^+ , Mg^{2+} , Al^{3+} , K^+ , Sr^{2+} , Mn^{2+} , Fe^{3+} , Fe^{2+} , Zn^{2+}) were examined by conventional peak reduction (PR)

technique. The mechanism of interference was explained by barrier width (BW) technique.

2 Materials and methods

2.1 Materials

Cadmium chloride, lead acetate, strontium nitrate, copper nitrate were procured from Rankem (India); aniline, chromium oxide, sodium arsenate salts were obtained from Loba Chemicals (Mumbai, India); zinc nitrate, sodium acetate, potassium ferrocyanide, magnesium chloride, aluminium chloride, potassium ferricyanide, potassium chloride were purchased from Fischer Scientific (USA); N-phenylglycine, ruthenium (III) chloride hydrate and cesium chloride were obtained from Sigma Aldrich (USA); sulfuric acid ($H_2SO_4 \cdot 6H_2O$) was procured from Qualigens (USA); diethylamine, di-sodium hydrogen phosphate and hydrochloric acid were obtained from Merck (Germany). The Uranium (VI) stock solution was purchased from S.P.Analytical, Navi Mumbai, India. Analytical grade chemicals were used in this work.

Double distilled water with conductivity lesser than $0.2 \mu S \text{ cm}^{-1}$ was used to prepare all the solutions. Auto-lab PGSTAT 302N, Eco chemie, The Netherlands, connected to a three-electrode cell with platinum wire as counter electrode, saturated Ag/AgCl as reference electrode was used to perform all the electrochemical experiments. The working electrode comprised a stainless steel (SS, 304) plate ($1.5 \text{ cm} \times 1 \text{ cm}$) of thickness 1 mm onto which the novel composite was electrodeposited. The SS 304 electrode was dipped to 0.5 cm into the electrolyte to maintain 1.5 cm^2 (i.e. both surfaces of $0.5 \text{ cm} \times 1.5 \text{ cm}$) as the effective surface area for all experiments. For all the electrochemical experiments the volume of the electrolytes was 50 ml.

2.2 Experimental methods

2.2.1 Synthesis and characterization of the novel composite film

The synthesis procedure for the novel composite film is similar to the synthesis of composite ANGO described in our previous works [48]. In this work, the novel composite was synthesized by chronopotentiometry at constant current of 2 mA cm^{-2} . For this purpose, 0.02 M aniline, 0.1 g N-phenylglycine, 0.1 g of GO and 0.1 g of p-tertbutylcalix[4]arene was taken in 1 M sulphuric acid solution. The amount of p-tertbutylcalix[4]arene was optimized by screening experiments. Since GO and p-terbutylcalix[4]arene were not soluble in 1 M sulphuric acid, therefore, the electrolyte 1 M sulphuric acid containing aniline, N-phenylglycine, GO and p-tertbutylcalix[4]arene was ultrasonicated for one hour

at room temperature for uniform dispersion. After deposition of the composite film, the electrodes were dried at 100 °C for 24 h in a vacuum oven. The dried sensing material was scraped out from the stainless-steel electrode surface for FTIR, FESEM and HRTEM analysis.

2.2.2 Material characterization

To verify the presence of the functional groups in the composite material, FTIR spectroscopy was performed at room temperature by using a Bruker (Vertex-70) FTIR spectroscope with thin pellets of KBr. The range of 4000–400 cm^{-1} was employed in the analysis with a resolution of 8 cm^{-1} . The surface morphology study of the composite films was conducted using a field emission scanning electron microscopy (FESEM) (Model MIRA3, TESCAN, USA). High resolution transmission electron microscopy (HRTEM) (Model FEI Titan G2 60–300 TEM, USA) was used to investigate the material structure.

2.2.3 Metal ion sensing

SWV experiments were performed to detect metal ions. For desired concentrations of uranyl ion (U^{6+}), uranium stock solution was used in electrolyte. To make desired ion concentrations of various test ions, ruthenium chloride hydrate (for Ru^{3+}), cesium chloride (for Cs^+), cadmium chloride (for Cd^{2+}), lead chloride (for Pb^{2+}), sodium arsenate (for As^{5+}), strontium nitrate (for Sr^+), copper nitrate (for Cu^{2+}), chromium oxide (for Cr^{6+}), sodium acetate (for Na^+), potassium chloride (for K^+), aluminium chloride (for Al^{3+}), potassium ferricyanide (for Fe^{3+}), zinc nitrate (for Zn^{2+}), potassium ferrocyanide (for Fe^{2+}), magnesium chloride (for Mg^{2+}) were used. All the metal ion solutions were prepared with an electrolyte of pH 3.3. Based on screening experiments, electrolyte pH 3.3 was decided. It was observed that the film can show better response at pH 2.5. The signal reduces as pH increases and shows minimum at pH 4.2. However, at pH 2–2.8, strong Pb^{2+} interference was observed which was possible to avoid at pH 3.3 or above. That is why pH 3.3 was chosen for metal ion sensing. To obtain the electrolyte solution, 0.1 M di-sodium-hydrogen phosphate was used as the base solution and a pH value of 3.3 was achieved after a gradual addition of 0.1 M hydrochloric acid.

To detect metal ions, the modified electrodes were immersed in the metal ion containing solution for 30 min which is regarded as the preconcentration step at open circuit potential. Next, the analyte was allowed to deposit on the electrode at a constant potential of 0.1 V for 200 s. SWV experiments were conducted in the potential window from 0.1 V to – 1.5 V. The various SWV parameters were, 0.1 V for amplitude, 0.075 V for the step potential and the frequency was maintained at 25 Hz. The LOD and sensitivity

values were extracted, and adsorption isotherms were plotted from which $-\Delta G_{\text{ads}}$ values were calculated.

2.2.4 Experiments to calculate barrier width

To calculate the barrier width, it is necessary to obtain the barrier height and charge transport resistance values [46, 73, 74]. For this purpose, CV experiments were performed to obtain the lowest unoccupied molecular orbital (LUMO) from which barrier height values were calculated (not shown here). The electrolyte was the same as in SWV experiment. 10 ppm concentration for U^{6+} was chosen as CV peaks were discernable at lower concentration of U^{6+} . To obtain the barrier heights of U^{6+} in presence of other test ions, a bicomponent salt solutions with 10 ppm of U^{6+} and a test ion at concentration of 20 ppm was used. For better interference analysis it is necessary to maintain higher concentration of the test ions than U^{6+} . The CV experiments were carried out at a potential window from – 1.5 V to 0.1 V with a scan rate of 100 mV s^{-1} .

Electrochemical impedance spectroscopy (EIS) experiments were performed for the film to obtain the charge transport resistances. A constant potential of 0.4 V was maintained, and a frequency range from 100 kHz to 1 Hz was used. The constant potential of 0.4 V was optimized by screening experiments. From the Nyquist plots obtained from EIS experiments, equivalent circuits were constructed from which charge transport resistances were evaluated. The electrolyte was maintained the same as in SWV experiments. For interference analysis bicomponent salt solution of U^{6+} and a test ion were chosen. The concentrations of U^{6+} and the test ions are mentioned in Sect. 3.3.2. *BW technique*. From the charge transport resistances and LUMO values, BW values were calculated.

2.2.5 CV for electroactive surface area

The electroactive surface area for the four different films were calculated from CV measurements using the Randles–Sevcik equation [75] (not shown here). These CV experiments were carried out with various sensing materials deposited on SS 304 electrode by chronopotentiometry (working) electrode, platinum counter electrode and Ag/AgCl reference electrodes at a potential window – 1.5 V to 1 V with the electrolyte being 0.1 M KCl containing 5 mM $[\text{Fe}(\text{CN})_6]^{-3/-4}$. The various sensing materials were (i) polyaniline, (ii) copolymer of aniline and N-phenylglycine, (iii) composite of aniline and GO, composite from aniline, N-phenylglycine and GO, (iv) aniline and GO and (v) the novel composite from aniline, N-phenylglycine, GO and p-tertbutylcalix-[4]-arene. The synthesis procedures of all these materials except the novel composite are described in our previous works [46, 48].

3 Results and discussion

3.1 Film synthesis and characterization

The film was deposited by chronopotentiometry at constant current of 2 mA cm^{-2} for 120 s onto the SS 304 electrode. The constant current deposition plot is shown in Fig. 1. In our one of the previous work [46], a novel composite from aniline and N-phenylglycine was synthesized by chronoamperometry, chronopotentiometry and cyclic voltammetry (CV). The film synthesized by chronopotentiometry had higher BET surface area as compared to the films synthesized by other two methods. It showed better response with lower LOD, higher sensitivity, higher Gibb's free energy of adsorption ($-\Delta G_{\text{ad}}$) than the films synthesized by chronoamperometry and CV. Therefore, in a subsequent work [48], another novel composite was synthesized by chronopotentiometry from aniline, N-phenylglycine and GO. In this work too, the same technique was employed due to its better performance. The constant current deposition of the films showed first an increasing trend and reached to the maximum at 16 s and then showed decreasing trend and then remained constant. This showed similar trend as synthesis of polyaniline, copolymer of aniline and N-phenylglycine [46] and composite named ANGO synthesized from aniline, N-phenylglycine and GO [48]. As mentioned in our previous work, for polyaniline, the peak was observed at 18 s, for copolymer the plot showed a peak at 52 s [46] and for the composite ANGO the peak was at 20 s [48]. The plot was compared with

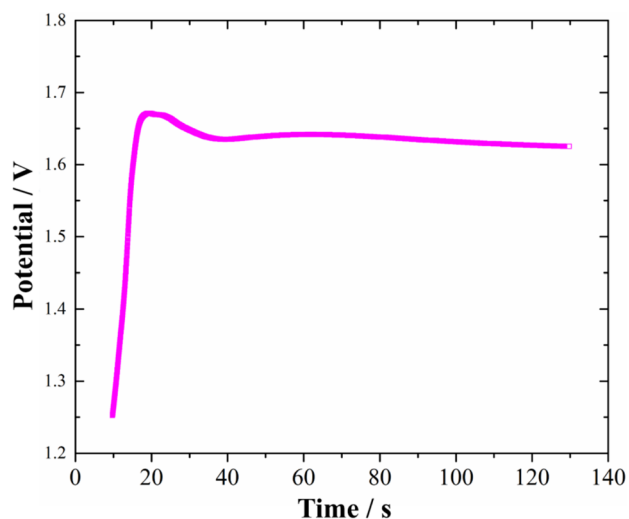


Fig. 1 A constant current deposition of the composite film synthesized from aniline, N-phenylglycine, GO and p-tertbutyl calix[4]arene on SS 304 electrode

chronopotentiometric deposition of polyaniline reported in literature [76] and it showed similar behaviour.

The FTIR characterization of the film is shown in Fig. 2a. For FTIR analysis, FTIR spectra of commercially available p-tertbutyl calix-[4]-arene was compared with the novel composite. For the FTIR spectra of p-tertbutyl calix-[4]-arene, the bands at 3235 cm^{-1} was due to OH and CH stretching vibrations. The bands around 3162 cm^{-1} was due to OH-stretching. At around 2937 cm^{-1} the bands were due to asymmetric C–H stretch of methylene groups. At around 2910 and 2865 cm^{-1} the bands were due to symmetric C–H vibrations of methyl and methylene groups respectively. Around 1610 , 1306 and 1258 cm^{-1} the bands were due to aromatic ring CC stretch and CCH bending. 1125 , 1029 and 977 cm^{-1} , the bands were due to aromatic C–H in plane bend. At 854 , 740 cm^{-1} the bands were due to aromatic C–H

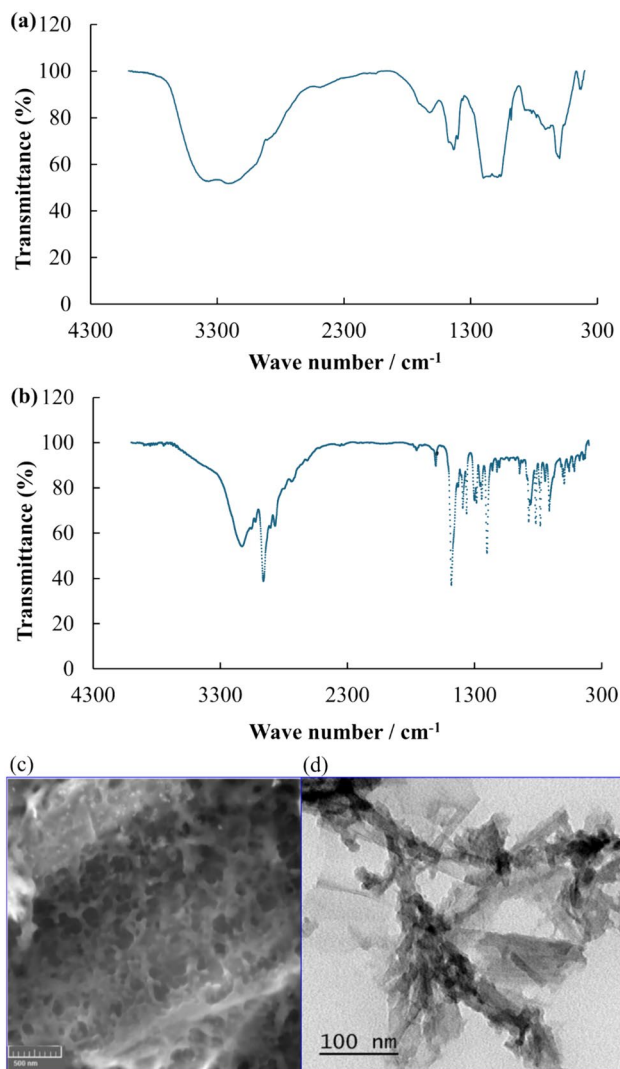


Fig. 2 FTIR of **a** the sensing material and **b** p-tertbutylcalix-[4]-arene; **c** FESEM and **d** HRTEM of the sensing material

and CC out of plane. CCC in plane bends were observed at 570 cm^{-1} [77, 78]. For the novel composite, the bands at around 1590 and 1496 cm^{-1} were due to stretching mode of quinoid and benzenoid rings of polymer. The peak at 1481 cm^{-1} and 1566 cm^{-1} were the qualitative measure of the oxidation process. The aromatic C-N vibration from quinoid and benzenoid ring was indicated by the peak at around 1310 cm^{-1} [79]. The spectra at 1666 cm^{-1} was due to the stretching mode of carbonyl in carboxyl groups [80]. These peaks indicate the presence of aniline and N-phenylglycine as mentioned in our previous work [46]. A broader band at 3339 cm^{-1} was due to stretching of C=O from GO. Peaks at 1230 and 1430 cm^{-1} were due to the presence of C-O from GO [81, 82]. The presence of p-tert butyl calix-[4]-arene was indicated by the presence of peak at 780 cm^{-1} which was due to aromatic C-H and CC out of plane band. At 550 cm^{-1} the peak was due to CCC in plane bend. Band at 1310 cm^{-1} was observed due to the aromatic ring CC stretch and CCH bending. Aromatic C-H in plane bend was observed at 1103 cm^{-1} . At 2950 and 2930 cm^{-1} the peaks are due to asymmetric C-H stretch of methyl group and asymmetric C-H stretch of methylene group respectively. A small peak for symmetric C-H vibration of methyl and methylene group were observed at 2897 and 2856 cm^{-1} respectively [78].

The FESEM image of composite film as shown in Fig. 2b shows tubular like structure embedded into GO matrix with an average diameter of $\sim 92\text{ nm}$. The structure is similar to the FESEM image of composite synthesized from aniline, N-phenylglycine and GO as reported in our previous work [48]. Since the sensing material is a novel material therefore it was not possible to find any literature for comparison with our FESEM results. However, the structure resembled the

composites synthesized from aniline and GO as reported in the literature [83, 84].

The HRTEM image of composite film in Fig. 2c showed sheet like structure where p-tertbutyl calix-[4] arene was tethered in GO sheet along with aniline and N-phenylglycine. The composite matrix contained GO which showed sheet like structure [48, 83, 85]. The dark patches indicated the presence of conducting polymers [48, 83, 85]. It showed similar structure as shown by composite synthesized from aniline, N-phenylglycine and GO as mentioned in our previous work [48]. We could not find any report where this composite is synthesized, therefore, we could not provide any comparison to support our HRTEM results.

3.2 Metal ion detection and thermodynamic analysis

SWV experiments were conducted to detect U^{6+} ions. A schematic of the detection procedure is shown in Fig. 3. The sensing material was deposited on stainless steel electrode as described earlier. The ligand to capture uranyl ion, p-tertbutylcalix-[4]-arene was embedded into the sensing matrix as well as into the sensing surface. The entire detection procedure can be described in three parts—pre-concentration at open circuit potential, preconcentration at 0.1 V followed by stripping of U^{6+} ion. As the preconcentration step at open circuit potential, the sensing electrodes were immersed in the aqueous ion containing solution for 30 min without applying any external voltage. Then a potential of 0.1 V was applied to deposit the ions into the electrode surface for 200 s . Following this, a square wave pulse was applied and the voltage was gradually decreased

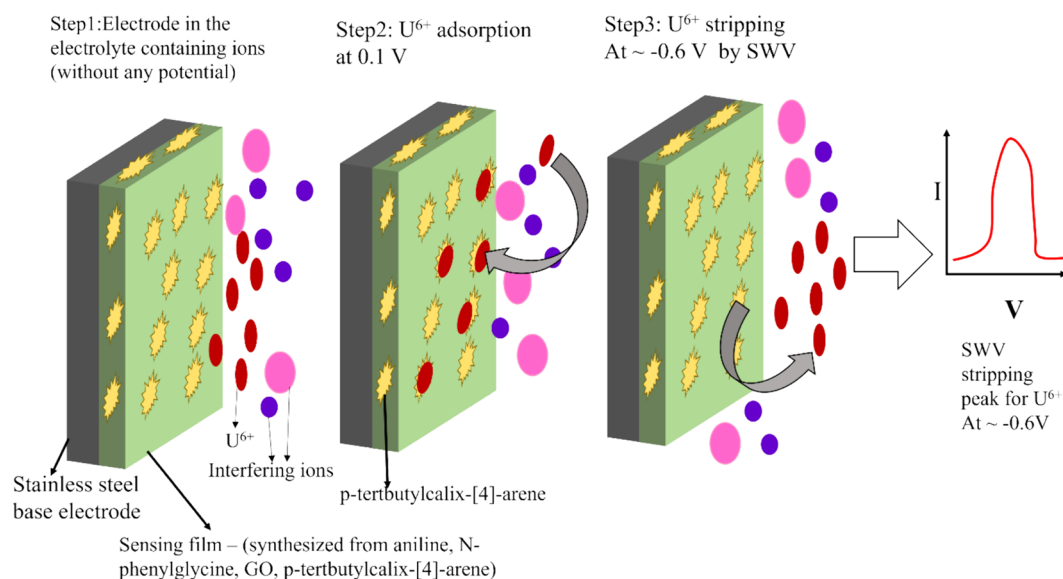


Fig. 3 Schematic of U^{6+} detection by square wave voltammetry by the composite film

to -1.5 V. At around -0.6 V, U^{6+} ions were stripped out and a peak for U^{6+} was observed. There are reports where stripping peak for U^{6+} was observed in the range -0.5 V to -0.6 V range and similar SWV profile was obtained. [86, 87]

Figure 4 shows the SWV plot for U^{6+} detection using the composite synthesized from aniline, N-phenylglycine and GO. The sensing material without p-tertbutyl calix[4]arene was able to detect U^{6+} till 10 ppm as there is no functional group or ligand attached to the surface to capture U^{6+} ion. That is why it is important to add a ligand in the sensing material such as p-tert butyl calix[4]arene so that it can capture U^{6+} ion at low concentration.

Using the composite synthesized from aniline, GO and p-tertbutyl calix[4]arene, LOD was 50 ppb. Using the novel sensing composite synthesized from aniline, N-phenylglycine, GO and p-tert butyl calix[4]arene, an LOD of 900 ppt (~ 2.27 nM) was achieved using this film electrode. The calibration plot was constructed, and the sensitivity of the system was found to be 0.201 mA [p [U^{6+}]] $^{-1}$. Figure 5a, b show the SWV plots and calibration plot for this system.

The adsorption isotherm was constructed to understand the interaction of the analyte to the electrode surface. The details regarding the construction of adsorption isotherms are explained in our previous works [46, 47], therefore not explained here. The adsorption isotherm for the film is shown in Fig. 6 from which $-\Delta G_{ads}$ value for the system was evaluated. For U^{6+} , the $-\Delta G_{ads}$ value was 60.750 kJ mol $^{-1}$ showing strong chemisorption. If the $-\Delta G_{ads}$ value for a process is higher than 40 kJ mol $^{-1}$, then chemisorption takes place due to the chemical reaction involved in between the electrode surface and the analyte of interest [88, 89].

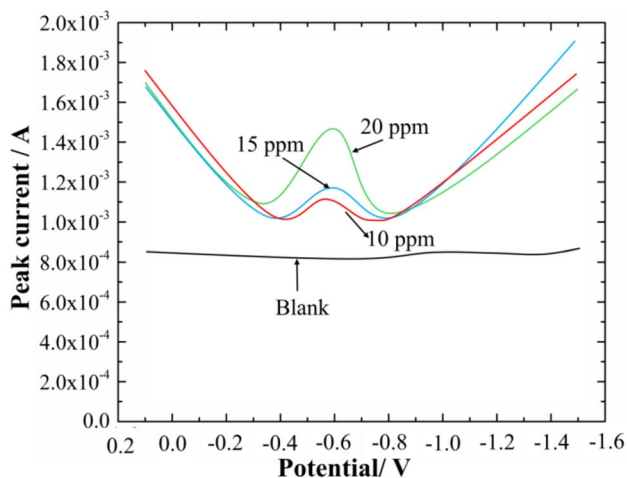


Fig. 4 SWV plot for different concentrations of U^{6+} using the composite synthesized from aniline, N-phenylglycine and GO

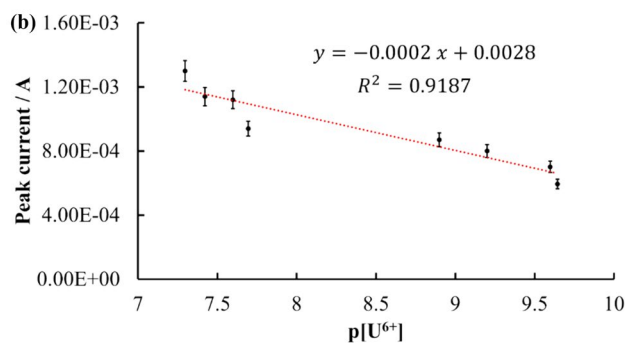
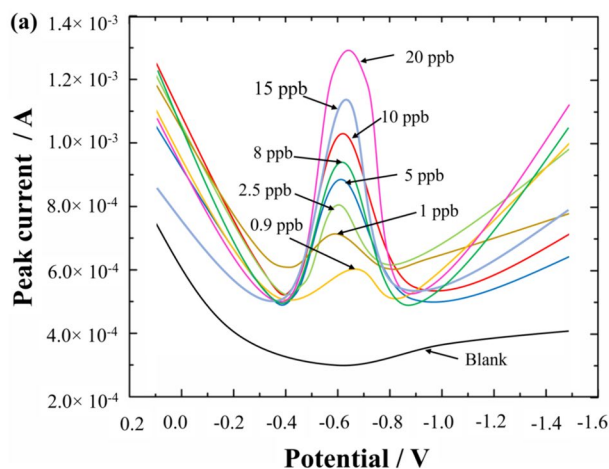


Fig. 5 a SWV plot for different concentrations of U^{6+} using the sensing material synthesized from aniline, N-phenylglycine, GO and p-tert butyl calix[4]arene b Calibration plot of the system

3.3 Interference study by peak reduction (PR) technique and barrier width (BW) technique

To conduct the interference study, both the techniques—PR technique as well as BW technique were employed with a number of test ions (Ru^{3+} , Cs^{+} , As^{5+} , Cr^{6+} , Cu^{2+} , Na^{+} , Mg^{2+} , Al^{3+} , K^{+} , Sr^{2+} , Mn^{2+} , Fe^{3+} , Fe^{2+} , Zn^{2+}). In each case

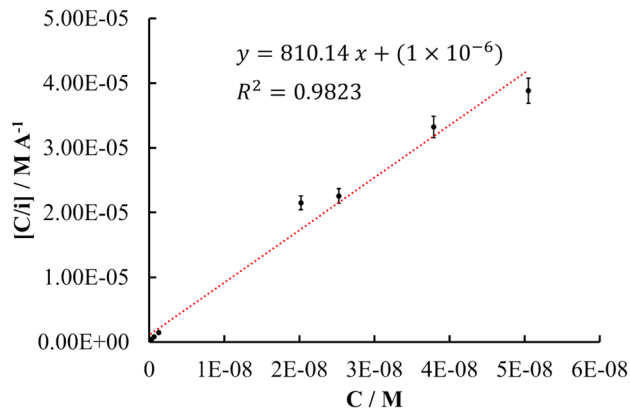


Fig. 6 Adsorption isotherm for the sensing film

a bicomponent solution with U^{6+} and one test ion in electrolyte solution of pH 3.3 was considered.

3.3.1 PR technique

For all the tests 4 ppb of U^{6+} was chosen. No interference was observed from 4 ppm of As^{5+} , Na^+ , Mg^{2+} , Al^{3+} , K^+ , Sr^{2+} , Mn^{2+} , Fe^{3+} , Fe^{2+} , Zn^{2+} to 4 ppb of U^{6+} . It was observed that 10 ppb of Cu^{2+} , Cr^{6+} reduces 4 ppb U^{6+} peak by 25–30% while 5–10% reduction in peak for 4 ppb of U^{6+} was observed in presence of 15 ppb Ru^{3+} and 25 ppb Cs^+ . In presence of 10 ppb of Cu^{2+} and Cr^{6+} each, the LOD was 4 ppb while in presence of 15 ppb of Ru^{3+} and 25 ppb of Cs^+ , the LOD was 3 ppb. To understand the mechanism of interference, BW technique was employed. The details of the PR technique are mentioned in Table 1.

p-tertbutyl calix-[4]-arene has been successfully used as macromolecular ligand to capture U^{6+} ion from water [90–92]. Duncan and Cockayne, have used a derivative of this ligand in PVC based ion selective electrodes for detection of U^{6+} from wastewater comprising a various number of anions and cations. The limit of detection was 1 ppm.

The limit of detection rises to 50 ppm with 10% waste background [90]. Gupta et al., have used commercially available p-tertbutylcalix-[4]-arene in PVC membrane for U^{6+} detection. They have checked the interference by fixed interference method and could detect U^{6+} till 3.9×10^{-5} M [91]. Ramirez et al., have used p-tertbutylcalix-[4]-arene in U^{6+} containing solution for its detection by optical means. They have checked the ligands ability if it can form complex with U^{6+} . Quantitative analysis for U^{6+} detection and interference analysis were not performed in that work [92]. We could not find any literature where polyaniline-based composite along with p-tert butylcalix[4]arene was used as sensing material for U^{6+} ion capture. However some comparisons were made where polyaniline or GO or p-tert butyl calix[4]arene based sensing material were used to detect U^{6+} ion as shown in Table 2.

From existing literature, it can be observed that only GO modified H_4L ion imprinted sensor can detect U^{6+} till 523 ppt level (Li et al., 2021 [96]). However, based on the existing literature, it can be concluded that the novel composite was able overcome interference to better extent than several sensors reported in the literature, and it could detect U^{6+} ion

Table 1 Interference results obtained from PR technique

Concentration of interfering species	U^{6+} concentration	Signal reduction	LOD in presence of interfering ion
4 ppm of As^{5+} , Na^+ , Mg^{2+} , Al^{3+} , K^+ , Sr^{2+} , Mn^{2+} , Fe^{3+} , Fe^{2+} , Zn^{2+}	4 ppb	No reduction in 4 ppb of U^{6+} signal	~3 ppb
10 ppb of Cu^{2+} , Cr^{6+}	4 ppb	25–30% reduction	4 ppb
15 ppb of Ru^{3+} and 25 ppb of Cs^+	4 ppb	5–10% reduction	3 ppb

Table 2 Comparison of different polyaniline or GO or calixarene based electrochemical sensor to detect U^{6+}

Authors & year	Sensing material	LOD for U^{6+}	Interference of different ions
Becker et al., 2008 [61]	4-sulfonic-calix[6]arene modified cystemine	1 μ M (~39.6 ppb)	Not mentioned
Duncan & Cockayne, 2001 [90]	5,11,17,23-tetra-tert-butyl-25,27-bis(hydroxy)-26-(ethoxycarbonylmethoxy)-28-(diethyl carbamoyl-methoxy) calix[4]arene modified PVC membrane	15 ppm	LOD for U^{6+} was 50 ppm in presence of 54 ppm Ca^{2+} , 38.7 ppm Na^+ and 135 ppm SO_4^{2-} in waste water
Ziotkowski et al., 2017 [93]	Carboxylated graphene	(5.0×10^{-8}) mol L^{-1} (~19.8 ppb)	Significant selectivity over Pb^{2+} , Cd^{2+} , Sr^{2+} , Mg^{2+} , Ca^{2+} , Fe^{3+} and Co^{2+}
Guo et al., 2022 [12]	Polydopamine/reduced GO modified glassy carbon electrode	0.05 μ mol L^{-1} (~19.8 ppb)	High selectivity over various ions (ions not mentioned)
Guo et al., 2020 [94]	Ag nanodendrite-reduced GO	0.85 μ M (~337 ppb)	Significant selectivity over 2 mM of Mg^{2+} , Ni^{2+} , Mg^{2+} , Co^{2+} , Zn^{2+} , Na^+ and Fe^{3+}
Gagandeep et al., 2022 [95]	Silica/polyaniline core shell nanocomposite membrane	(1.4×10^{-7}) M (~55.8 ppb)	No significant interference in real sample
Li et al., 2021 [96]	GO modified H_4L ion imprinted sensor	1.32 nM (~523 ppt)	Tested with real sample, no significant interference

in drinking water with a limit of detection of 4 ppb in presence of highly interfering species.

The sensor was used to detect U^{6+} in three commercially available packaged drinking water and tap water. It was successful in detecting U^{6+} with no significant interference.

3.3.2 BW technique

BW technique was employed to understand the underlying mechanism of the interference analysis conducted by PR technique. A detailed description of the methodology of the BW technique based on Simmon's model is illustrated in our previous works [46, 47], not explained here. To calculate the barrier width for charge transport, following equation was used.

$$R_{ct} = R_{ct0} \exp(\beta d) \quad (1)$$

[46, 73, 74]

$$\beta = \sqrt{\frac{2m_e\phi}{\hbar^2}} \quad (2)$$

[46, 73, 74]

Where, R_{ct} denotes the charge transport resistance of U^{6+} , R_{ct0} is the charge transport resistance in blank electrolyte solution, d is the barrier width, β is the tunnelling constant calculated from Eq. (2), m_e is the mass of electron, ϕ is the Barrier height (extracted from LUMO) and \hbar is the Planck's constant. Using CV and EIS, barrier width values were calculated. To calculate the barrier height, first the LUMO values were calculated as described in our previous work [46] and from these values barrier height values were evaluated [97–100].

To perform EIS experiments the concentrations of U^{6+} and the interfering ions were same as mentioned in Table 1. From the EIS experiments Nyquist plots were obtained for each of the bicomponent solution case from which equivalent circuit was constructed. Figure 7 shows the experimental Nyquist plot obtained from EIS experiment for 4 ppb of U^{6+} . The equivalent circuit fitted to the plot is shown in inset of Fig. 7. The equivalent circuit consists of four elements – solution resistance R_s , charge transport resistance R_{ct} , double layer capacitance C_{DL} and Warburg impedance W . From the LUMO values obtained from CV and R_{ct} values from EIS, the barrier width values for different cases were calculated. The barrier width for U^{6+} was 0.244 Å. Table 3 shows the barrier width values for U^{6+} in presence of interference species. No change in d values were observed to 4 ppb concentration of U^{6+} in presence of 4 ppm of As^{5+} , Na^+ , Mg^{2+} , Al^{3+} , K^+ , Sr^{2+} , Mn^{2+} , Fe^{3+} , Fe^{2+} , Zn^{2+} .

From Table 2 it can be observed that presence of 10 ppb of Cr^{6+} and Cu^{2+} , each, increases the d value to almost 5 times raising hindrance to charge transfer and decreasing

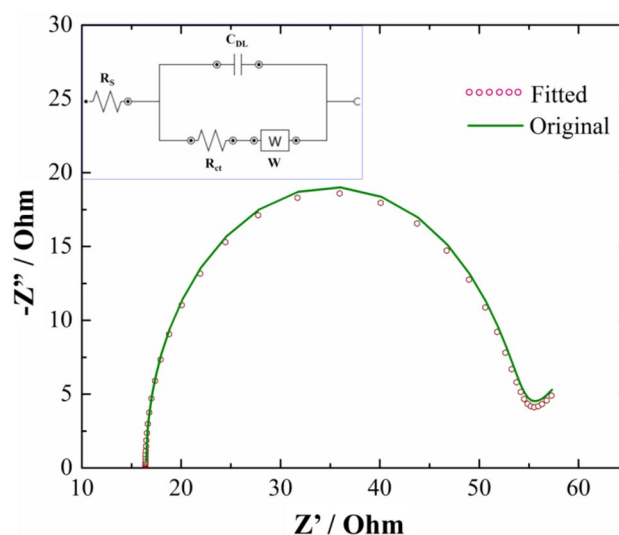


Fig. 7 Nyquist plot obtained for the film in presence of 4 ppb of U^{6+} in electrolyte solution of pH 3.3 –experimental (solid line) and fitted to the equivalent circuit (symbol) (inset—equivalent circuit)

Table 3 Parameters obtained from BW technique

Metal ions	Concentration of U^{6+} (ppb)	Concentration of interfering ion (ppb)	Barrier width (d) (Å)
$U^{6+} + Cr^{6+}$	4	10	1.126
$U^{6+} + Cu^{2+}$	4	10	1.221
$U^{6+} + Ru^{3+}$	4	15	0.387
$U^{6+} + Cs^+$	4	25	0.394

the sensing signal by 25–30%. Comparative to them, presence of Ru and Cs increases it to almost 1.5 times leading to 5–10% reduction in sensing signal. Therefore, the barrier width value supports the analysis made by PR technique.

3.4 Calculation of the electro-active surface area of the novel composite film

Electroactive surface area is a key factor which has a strong influence in selectivity and sensing. Therefore, to investigate the reason behind the good sensitivity and selectivity of the novel composite, the electroactive surface area of the film was calculated and compared with the films synthesized from (i) aniline, (ii) aniline-N-phenylglycine, (iii) aniline-GO and (iv) aniline-N-phenylglycine –GO as described in our previous works [46, 47]. All the films were synthesized by chronopotentiometry. The film thicknesses were maintained at 12 μm . CV was performed with electrolyte containing 5 mM $[Fe(CN)_6]^{-3/-4}$ in 0.1 M KCl. To calculate the electroactive surface area, the Randles–Sevcik equation [75],

Table 4 Comparison of the different electrodes based on their electro-active surface area

Film synthesized from	Electro-active surface area (cm ²)
(i) Aniline	0.209
(ii) Aniline and N-phenylglycine	0.376
(iii) Aniline and GO	0.287
(iv) Aniline, N-phenylglycine and GO	0.496
(v) Aniline, N-phenylglycine, GO and p-tertbutyl-calix-[4]-arene	0.651

$$I_p = 2.69 \times 10^5 A \times D^{1/2} n^{2/3} C v^{1/2} \quad (3)$$

was used where, I_p denotes the maximum current in Amp, A is the electrode area (1.5 cm²), D is the diffusion coefficient of Fe(CN)₆^{-3/-4} solution (7.6×10^{-6} cm² s⁻¹) [101] in cm² s⁻¹ (in our case similar value was obtained), n is the number of electron transferred (here $n = 1$), C is the concentration in mol cm⁻³ (5 mM) and v is the scan rate in mV s⁻¹. The electroactive surface area of all the films are mentioned in Table 4.

From Table 3 it is clear that the electroactive surface area of the novel composite electrode was the highest as compared with other electrodes which makes it enable for maximum U⁶⁺ ion intake. The advantage of the novel composite lies in its synthesis procedure and can be used as it does not require any surface modification for U⁶⁺ detection and it can overcome interference to a great extent.

4 Conclusion

In this work, a novel composite was synthesized from aniline, N-phenylglycine, GO and p-tertbutylcalix[4]arene. SWV experiments to detect U⁶⁺ were performed and LOD of 900 ppt (~2.273 nM) was obtained. The sensitivity of the film was 0.201 mA [p[U⁶⁺]]⁻¹. To understand the interaction of the analyte to the electrode surface, thermodynamic analysis was carried out. Adsorption isotherm was constructed and $-\Delta G_{ads}$ value was found to be 60.750 kJ mol⁻¹ indicating a strong chemisorption process. Interference study was carried out with a large number of test ions (Ru³⁺, Cs⁺, As⁵⁺, Cr⁶⁺, Cu²⁺, Na⁺, Mg²⁺, Al³⁺, K⁺, Sr²⁺, Mn²⁺, Fe³⁺, Fe²⁺, Zn²⁺) by both PR technique and BW technique. The PR technique showed that only Ru³⁺, Cs⁺, Cr⁶⁺ and Cu²⁺ interferes U⁶⁺ detection in both the cases. 10 ppb concentration of Cr⁶⁺, Cu²⁺ each shows 25–30% reduction in sensing signal while a 5–10% decrease in sensing signal was observed in presence of 15 ppb Ru³⁺ and 25 ppb Cs⁺ each. To understand the mechanism of interference BW technique was used. It was observed that the barrier width for only U⁶⁺

was 0.244 Å. In presence of 10 ppb of Cu²⁺ and Cr⁶⁺ each it increases to 1.126 and 1.221 Å respectively. In presence of 15 ppb Ru³⁺ and 25 ppb Cs⁺, the BW value of U⁶⁺ changes to 0.387 and 0.394 Å respectively. Therefore, BW technique results support the results obtained by PR technique. The sensing material synthesized in this work has been used for the first time for uranyl ion detection with less interference has the advantage in ease in synthesis procedure requiring no surface modification and leading to a LOD of 4 ppb for U⁶⁺ in presence of interfering ions, which is far below the permissible limit for U⁶⁺ in drinking water.

Acknowledgements The authors would like to acknowledge Bhaba Atomic Research Centre, Mumbai, India and Dr. Tessa Vincent, Senior Scientist, Process Development Division, Nuclear Recycle Group, BARC, Mumbai, India for providing unconditional support for conducting this research work.

Author contributions Both the authors Dr. Kusumita Dutta and Prof. Siddhartha Panda contributed to the study, conception and design. Material preparation, data collection and analysis were performed by Dr. Kusumita Dutta. The first draft of the manuscript was written by Dr. Kusumita Dutta. Both the authors Dr. Kusumita Dutta and Prof. Siddhartha Panda were involved in review, analysis and correction of the manuscript. Both the authors read and approved the final manuscript.

Funding The authors acknowledge the financial support from the Ministry of Electronics and Information Technology, Government of India (grant number 2(4)/2014-PEGD (IPIIW)).

Declarations

Competing interests There is no competing interest.

Ethical approval Not Applicable.

Consent to participate The corresponding author is free to contact the co-author involved in this research to seek further clarification and information.

Consent for publication Not Applicable.

References

- Vellingiri B (2023) A deeper understanding about the role of uranium toxicity in neurodegeneration. *Environ Res* 233:116430. <https://doi.org/10.1016/j.envres.2023.116430>
- Daniel R, Tripathi D, Singh S et al (2022) Uranium: occurrence, distribution across India and its potential health effects. *J Radioanal Nucl Chem* 331:2805–2815. <https://doi.org/10.1007/s10967-022-08373-3>
- Zhang L, Chu J, Xia B et al (2022) Health effects of particulate uranium exposure. *Toxics* 10:575. <https://doi.org/10.3390/toxics10100575>
- Zhou Z, Zhou Y, Liang X et al (2019) Sensitive detection of uranium in water samples using differential pulse adsorptive stripping voltammetry on glassy carbon electrode. *J Radioanal Nucl Chem* 322:2049–2056. <https://doi.org/10.1007/s10967-019-06892-0>

5. Zhang L, Wang C-Z, Tang H-B et al (2015) Rapid determination of uranium in water samples by adsorptive cathodic stripping voltammetry using a tin-bismuth alloy electrode. *Electrochim Acta* 174:925–932. <https://doi.org/10.1016/j.electacta.2015.06.087>
6. Hindin R, Brugge D, Panikkar B (2005) Teratogenicity of depleted uranium aerosols: A review from an epidemiological perspective. *Environ Health*. <https://doi.org/10.1186/1476-069X-4-17>
7. Sawant LR, Kalsi PK, Kulkarni AV, Vaidyanathan S (1996) Differential pulse voltammetric determination of uranium in low concentration streams. *J Radioanal Nucl Chem Art* 207:39–43. <https://doi.org/10.1007/BF02036523>
8. Andreotti E, Credaro A, Dossi C et al (2008) Determination of uranium content in water using cathodic stripping voltammetry and gamma-spectrometry. *J Radioanal Nucl Chem* 277:413–417. <https://doi.org/10.1007/s10967-007-7018-1>
9. Geça I, Korolczuk M (2023) A novel eco-friendly and highly sensitive solid lead-tin microelectrode for trace U(VI) determination in natural water samples. *Sensors* 23:2552. <https://doi.org/10.3390/s23052552>
10. Bou-Rabee F, Bakir Y, Bem H (1995) Contribution of uranium to gross alpha radioactivity in some environmental samples in Kuwait. *Environ Int* 21:293–298. [https://doi.org/10.1016/0160-4120\(95\)00022-D](https://doi.org/10.1016/0160-4120(95)00022-D)
11. Bagatti D, Cantone MC, Giussani A et al (2003) Regional dependence of urinary uranium baseline levels in non-exposed subjects with particular reference to volunteers from Northern Italy. *J Environ Radioact* 65:357–364. [https://doi.org/10.1016/S0265-931X\(02\)00107-8](https://doi.org/10.1016/S0265-931X(02)00107-8)
12. Guo W, Xu H, Chen C et al (2022) Determination of U(VI) by differential pulse stripping voltammetry using a polydopamine/reduced graphene oxide nanocomposite modified glassy carbon electrode. *Microchem J* 175:107111. <https://doi.org/10.1016/j.microc.2021.107111>
13. Brugge D, Buchner V (2011) Health effects of uranium: new research findings. *Rev Environ Health* 26:231–249. <https://doi.org/10.1515/REVEH.2011.032>
14. Arfsten DP, Still KR, Ritchie GD (2001) A review of the effects of uranium and depleted uranium exposure on reproduction and fetal development. *Toxicol Ind Health* 17:180–191. <https://doi.org/10.1191/0748233701th1110a>
15. Kreuzer M, Sommer M, Deffner V et al (2024) Lifetime excess absolute risk for lung cancer due to exposure to radon: results of the pooled uranium miners cohort study PUMA. *Radiat Environ Biophys*. <https://doi.org/10.1007/s00411-023-01049-w>
16. Zupunski L, Street R, Ostroumova E et al (2023) Environmental exposure to uranium in a population living in close proximity to gold mine tailings in South Africa. *J Trace Elem Med Biol* 77:127141. <https://doi.org/10.1016/j.jtemb.2023.127141>
17. Bajwa BS, Kumar S, Singh S et al (2017) Uranium and other heavy toxic elements distribution in the drinking water samples of SW-Punjab, India. *J Radiat Res Appl Sci* 10:13–19. <https://doi.org/10.1016/j.jrras.2015.01.002>
18. Coyte RM, Jain RC, Srivastava SK et al (2018) Large-scale uranium contamination of groundwater resources in India. *Environ Sci Technol Lett* 5:341–347. <https://doi.org/10.1021/acs.estlett.8b00215>
19. Balaran V, Rani A, Rathore DPS (2022) Uranium in groundwater in parts of India and world: a comprehensive review of sources, impact to the environment and human health, analytical techniques, and mitigation technologies. *Geosystems and Geoenvironment* 1:100043. <https://doi.org/10.1016/j.geogeo.2022.100043>
20. Sharma AD, Rishi MS (2016) Presence of uranium in groundwater of punjab: an overview. *Geostatistical and geospatial approaches for the characterization of natural resources in the environment*. Springer International Publishing, Cham, pp 231–236
21. Alam MdS, Cheng T (2014) Uranium release from sediment to groundwater: Influence of water chemistry and insights into release mechanisms. *J Contam Hydrol* 164:72–87. <https://doi.org/10.1016/j.jconhyd.2014.06.001>
22. Pant D, Keesari T, Roy A et al (2019) Study on groundwater quality in parts of Rajasthan with special reference to uranium contamination. *J Radioanal Nucl Chem* 322:165–171. <https://doi.org/10.1007/s10967-019-06525-6>
23. MacDonald AM, Bonsor HC, Ahmed KM et al (2016) Groundwater quality and depletion in the Indo-Gangetic Basin mapped from in situ observations. *Nat Geosci* 9:762–766. <https://doi.org/10.1038/ngeo2791>
24. Brindha K, Elango L (2013) Occurrence of uranium in groundwater of a shallow granitic aquifer and its suitability for domestic use in southern India. *J Radioanal Nucl Chem* 295:357–367. <https://doi.org/10.1007/s10967-012-2090-6>
25. Singh KP, Kishore N, Tuli N et al (2018) Uranium contamination of groundwater in southwest parts of Punjab state, India, with special reference to role of basement granite. Springer, Cham, pp 95–106
26. Alrakabi M, Singh G, Bhalla A et al (2012) Study of uranium contamination of ground water in Punjab state in India using X-ray fluorescence technique. *J Radioanal Nucl Chem* 294:221–227. <https://doi.org/10.1007/s10967-011-1585-x>
27. Kumar M, Rathore DPS, Singh AK (2001) Pyrogallol immobilized amberlite XAD-2: a newly designed collector for enrichment of metal ions prior to their determination by flame atomic absorption spectrometry. *Microchim Acta* 137:127–134. <https://doi.org/10.1007/s006040170002>
28. Avivar J, Ferrer L, Casas M, Cerdà V (2010) Automated determination of uranium(VI) at ultra trace levels exploiting flow techniques and spectrophotometric detection using a liquid waveguide capillary cell. *Anal Bioanal Chem* 397:871–878. <https://doi.org/10.1007/s00216-010-3600-4>
29. Krishna MVB, Arunachalam J (2004) Ultrasound-assisted extraction procedure for the fast estimation of major, minor and trace elements in lichen and mussel samples by ICP-MS and ICP-AES. *Anal Chim Acta* 522:179–187. <https://doi.org/10.1016/j.aca.2004.07.006>
30. Kumar SA, Shenoy NS, Pandey S et al (2008) Direct determination of uranium in seawater by laser fluorimetry. *Talanta* 77:422–426. <https://doi.org/10.1016/j.talanta.2008.07.002>
31. Misra NL, Dhara S, Mudher KDS (2006) Uranium determination in seawater by total reflection X-ray fluorescence spectrometry. *Spectrochim Acta Part B At Spectrosc* 61:1166–1169. <https://doi.org/10.1016/j.sab.2006.05.002>
32. Cho H-R, Jung EC, Cha W, Song K (2013) Quantitative analysis of uranium in aqueous solutions using a semiconductor laser-based spectroscopic method. *Anal Chem* 85:4279–4283. <https://doi.org/10.1021/ac303752t>
33. Jamali MR, Assadi Y, Shemirani F et al (2006) Synthesis of salicylaldehyde-modified mesoporous silica and its application as a new sorbent for separation, preconcentration and determination of uranium by inductively coupled plasma atomic emission spectrometry. *Anal Chim Acta* 579:68–73. <https://doi.org/10.1016/j.aca.2006.07.006>
34. Chandrasekaran K, Karunasagar D, Arunachalam J (2011) Dispersive liquid–liquid micro extraction of uranium(vi) from groundwater and seawater samples and determination by inductively coupled plasma–optical emission spectrometry and flow injection–inductively coupled plasma mass spectrometry. *Anal Methods* 3:2140. <https://doi.org/10.1039/c1ay05329a>

35. Boryło A (2013) Determination of uranium isotopes in environmental samples. *J Radioanal Nucl Chem* 295:621–631. <https://doi.org/10.1007/s10967-012-1900-1>
36. Ariño C, Banks CE, Bobrowski A et al (2022) Electrochemical stripping analysis. *Nat Rev Methods Prim* 2:62. <https://doi.org/10.1038/s43586-022-00143-5>
37. Rahn KL, Peramune U, Zhang T, Anand RK (2023) Label-free electrochemical methods for disease detection. *Annu Rev Anal Chem* 16:49–69. <https://doi.org/10.1146/annurev-anchem-091622-085754>
38. Baranwal J, Barse B, Gatto G et al (2022) Electrochemical sensors and their applications: a review. *Chemosensors* 10:363. <https://doi.org/10.3390/chemosensors10090363>
39. Wu J, Liu H, Chen W et al (2023) Device integration of electrochemical biosensors. *Nature Rev Bioeng* 1:346–360. <https://doi.org/10.1038/s44222-023-00032-w>
40. Zhang L, Guo W, Lv C et al (2023) Electrochemical biosensors represent promising detection tools in medical field. *Adv Sensor Energy Mater* 2:100081. <https://doi.org/10.1016/j.asems.2023.100081>
41. Grabarczyk M, Koper A (2013) Simultaneous quantification of Bi(III) and U(VI) in environmental water samples with a complicated matrix containing organic compounds. *Environ Monit Assess* 185:5515–5522. <https://doi.org/10.1007/s10661-012-2963-8>
42. Maheshwaran M, Satheesh Kumar KK (2024) DFT and electrochemical determination of Hg²⁺ and Pb²⁺ in water using polyaniline–quinoxaline composite modified GCE electrode. *J Mol Liq*. <https://doi.org/10.1016/j.molliq.2024.124317>
43. Jose J, Prakash P, Jeyaprabha B et al (2023) Principle, design, strategies, and future perspectives of heavy metal ion detection using carbon nanomaterial-based electrochemical sensors: a review. *J Iran Chem Soc* 20:775–791. <https://doi.org/10.1007/s13738-022-02730-5>
44. Yao C, Sun H, Zhang Y et al (2023) Polyaniline nanoflowers-based electrochemical sensor for sensitive and reliable detection of copper ion. *Russ J Gen Chem* 93:S1006–S1015. <https://doi.org/10.1134/S1070363223170164>
45. Wang N, Huang S, Cai H et al (2023) In-situ synthesis of bimetallic metal organic Framework/Polyaniline nanocomposites as ultrasensitive and selective electrodes for electrochemical detection of heavy metal ions. *Microchem J* 193:109185. <https://doi.org/10.1016/j.microc.2023.109185>
46. Dutta K, Panda S (2018) Identification of the levels of interference of ions toward heavy metal detection in electrochemical sensors using the barrier width technique. *J Electrochem Soc* 165:B378. <https://doi.org/10.1149/2.1331809jes>
47. Dutta K, Panda S (2018) Interference analysis for electrochemical heavy metal ion sensors in terms of stripping current, barrier width and adsorption. *J Electrochem Soc* 165:B644. <https://doi.org/10.1149/2.1071813jes>
48. Dutta K, Panda S (2019) Thermodynamic and charge transport studies for the detection of heavy metal ions in electrochemical sensors using a composite film of aniline, N-phenylglycine and graphene oxide. *J Electrochem Soc* 166:B1335. <https://doi.org/10.1149/2.1151914jes>
49. Lei X, Su Z (2007) Novel conducting polyaniline copolymers of aniline and N-phenylglycine. *Mater Lett* 61:1158–1161. <https://doi.org/10.1016/j.matlet.2006.06.076>
50. Abbasi Sh, Sohrabi A, Naghipour A et al (2008) Determination of ultra trace amounts of uranium (VI) by adsorptive stripping voltammetry using L-3-(3, 4-dihydroxy phenyl) alanine as a selective complexing agent. *Anal Lett* 41:1128–1143. <https://doi.org/10.1080/00032710802051967>
51. Wang J, Setiadji R, Chen L et al (1992) Automated system for on-line adsorptive stripping voltammetric monitoring of trace levels of uranium. *Electroanalysis* 4:161–165. <https://doi.org/10.1002/elan.1140040206>
52. Sander S (1999) Simultaneous adsorptive stripping voltammetric determination of molybdenum(VI), uranium(VI), vanadium(V), and antimony(III). *Anal Chim Acta* 394:81–89. [https://doi.org/10.1016/S0003-2670\(99\)00218-4](https://doi.org/10.1016/S0003-2670(99)00218-4)
53. Kadi MW, El-Shahawi MS (2009) Differential pulse cathodic stripping voltammetric determination of uranium with arsenazo-III at the hanging mercury dropping electrode. *Radiochim Acta* 97:613–620. <https://doi.org/10.1524/ract.2009.1659>
54. Ali AMM, Ghandour MA, Khodari M (1995) Adsorptive stripping voltammetric determination of uranium with cephradine. *Analyst* 120:1065–1068. <https://doi.org/10.1039/an9952001065>
55. Pournaghi-Azar MH, Zargharian R (1996) Adsorptive pulse polarographic determination of uranium(VI) oxinate in chloroform and its use for the analysis of uranium mineral ores. *Anal Chim Acta* 328:33–39. [https://doi.org/10.1016/0003-2670\(96\)00064-5](https://doi.org/10.1016/0003-2670(96)00064-5)
56. Wang J, Lu J, Luo D et al (1997) Simultaneous adsorptive stripping voltammetric measurements of trace chromium, uranium, and iron in the presence of cupferron. *Electroanalysis* 9:1247–1251. <https://doi.org/10.1002/elan.1140091606>
57. Lin L, Thongngamdee S, Wang J et al (2005) Adsorptive stripping voltammetric measurements of trace uranium at the bismuth film electrode. *Anal Chim Acta* 535:9–13. <https://doi.org/10.1016/j.aca.2004.12.003>
58. Kefala G, Economou A, Voulgaropoulos A (2004) A study of Nafion-coated bismuth-film electrodes for the determination of trace metals by anodic stripping voltammetry. *Analyst* 129:1082–1090. <https://doi.org/10.1039/b404978k>
59. Gholivand M, Nassab H, Fazeli H (2005) Cathodic adsorptive stripping voltammetric determination of uranium (VI) complexed with 2, 6-pyridinedicarboxylic acid. *Talanta* 65:62–66. <https://doi.org/10.1016/j.talanta.2004.05.019>
60. Dimovasilis PA, Prodromidis MI (2011) An electrochemical sensor for trace uranium determination based on 6-O-palmitoyl-L-ascorbic acid-modified graphite electrodes. *Sens Actuators B Chem* 156:689–694. <https://doi.org/10.1016/j.snb.2011.02.019>
61. Becker A, Tobias H, Porat Z, Mandler D (2008) Detection of uranium(VI) in aqueous solution by a calix[6]arene modified electrode. *J Electroanal Chem* 621:214–221. <https://doi.org/10.1016/j.jelechem.2007.11.009>
62. Betelu S, Vautrin-UI C, Chaussé A (2009) Novel 4-carboxy-phenyl-grafted screen-printed electrode for trace Cu(II) determination. *Electrochem Commun* 11:383–386. <https://doi.org/10.1016/j.elecom.2008.11.035>
63. Yantasee W, Lin Y, Fryxell GE, Wang Z (2004) Carbon paste electrode modified with carbamoylphosphonic acid functionalized mesoporous silica: a new mercury-free sensor for uranium detection. *Electroanalysis* 16:870–873. <https://doi.org/10.1002/elan.200302868>
64. Yun C, Hwang S (2021) Analysis of the charging current in cyclic voltammetry and supercapacitor's galvanostatic charging profile based on a constant-phase element. *ACS Omega* 6:367–373. <https://doi.org/10.1021/acsomega.0c04702>
65. Bala A, Rebiś J, Górski Ł (2017) Phosphorothioated oligonucleotides as receptor layers in electrochemical detection of uranyl cation. *J Electrochem Soc* 164:B470–B475. <https://doi.org/10.1149/2.1671709jes>
66. Guo H, Yang F, Chai X et al (2012) Synthesis of novel calix[6]-1,4-crown-based netty polymer and its excellent adsorption capabilities for aniline derivatives. *Iran Polym J* 21:455–451. <https://doi.org/10.1007/s13726-012-0048-8>
67. Mohammadi A, Lakouraj MM, Barikani M (2014) Preparation and characterization of p-tert-butyl thiocalix[4]arene imbedded flexible polyurethane foam: an efficient novel cationic dye

- adsorbent. *React Funct Polym* 83:1353–1361. <https://doi.org/10.1016/j.reactfunctpolym.2014.07.003>
68. Mohammadi A, Doctorsafaei AH, Zia KM (2018) Alginate/calix[4]arenes modified graphene oxide nanocomposite beads: preparation, characterization, and dye adsorption studies. *Int J Biol Macromol* 120:14–23. <https://doi.org/10.1016/j.ijbiomac.2018.09.136>
69. Zhang P, Wang Y, Zhang D et al (2016) Calixarene-functionalized graphene oxide composites for adsorption of neodymium ions from the aqueous phase. *RSC Adv* 6:30384–30394. <https://doi.org/10.1039/C5RA27509A>
70. Gutsche CD, Iqbal M, Stewart D (1986) Calixarenes. 19. synthesis procedures for p-tert-butylcalix[4]arene. *J Org Chem* 51:742–745. <https://doi.org/10.1021/jo00355a033>
71. Hyder A, Thebo M, Janwery D et al (2023) Fabrication of para-dimethylamine calix[4]arene functionalized self-assembled graphene oxide composite material for effective removal of 2, 4, 6-tri-chlorophenol from aqueous environment. *Heliyon* 9:e19622. <https://doi.org/10.1016/j.heliyon.2023.e19622>
72. Wu Y, Chen K, Wang F (2023) C-undecylcalix[4]resorcinarene langmuir–blodgett/porous reduced graphene oxide composite film as a electrochemical sensor for the determination of tryptophan. *Biosensors (Basel)* 13:1024. <https://doi.org/10.3390/bios13121024>
73. Bradbury CR, Zhao J, Fermín DJ (2008) Distance-independent charge-transfer resistance at gold electrodes modified by thiol monolayers and metal nanoparticles. *J Phys Chem C* 112:10153–10160. <https://doi.org/10.1021/jp710165d>
74. Zhao J, Bradbury CR, Huclova S et al (2005) Nanoparticle-mediated electron transfer across ultrathin self-assembled films. *J Phys Chem B* 109:22985–22994. <https://doi.org/10.1021/jp054127s>
75. Song M-J, Hwang SW, Whang D (2010) Amperometric hydrogen peroxide biosensor based on a modified gold electrode with silver nanowires. *J Appl Electrochem* 40:2099–2105. <https://doi.org/10.1007/s10800-010-0191-x>
76. Cheraghi B, Fakhari AR, Borhani S, Entezami AA (2009) Chemical and electrochemical deposition of conducting polyaniline on lead. *J Electroanal Chem* 626:116–122. <https://doi.org/10.1016/j.jelechem.2008.11.011>
77. Griffiths PR, de Haseth JA (2007) Fourier transform infrared spectrometry. Wiley, New York
78. Furer VL, Borisoglebskaya EI, Zverev VV, Kovalenko VI (2005) The hydrogen bonding and conformations of p-tert-butylcalix[4]arene as studied by IR spectroscopy and by DFT calculations. *Spectrochim Acta A Mol Biomol Spectrosc* 62:483–493. <https://doi.org/10.1016/j.saa.2005.02.001>
79. Jeevananda T, Siddaramaiah SS et al (2004) Synthesis and characterization of poly (aniline-co-acrylonitrile) using organic benzoyl peroxide by inverted emulsion method. *Synth Met* 140:247–260. [https://doi.org/10.1016/S0379-6779\(03\)00366-7](https://doi.org/10.1016/S0379-6779(03)00366-7)
80. Euler WB (1986) Extended Huckel calculations on the Pi system of polyaniline. *Solid State Commun* 57:857–859. [https://doi.org/10.1016/0038-1098\(86\)90166-3](https://doi.org/10.1016/0038-1098(86)90166-3)
81. Zaaba NI, Foo KL, Hashim U et al (2017) Synthesis of graphene oxide using modified hummers method: solvent influence. *Procedia Eng* 184:469–477. <https://doi.org/10.1016/j.proeng.2017.04.118>
82. Cao N, Zhang Y (2015) Study of reduced graphene oxide preparation by hummers' method and related characterization. *J Nanomater* 2015:1–5. <https://doi.org/10.1155/2015/168125>
83. Asen P, Shahrokhian S, zad AI, (2018) Ternary nanostructures of Cr₂O₃/graphene oxide/conducting polymers for supercapacitor application. *J Electroanal Chem* 823:505–516. <https://doi.org/10.1016/j.jelechem.2018.06.048>
84. Xu J, Wang K, Zu S-Z et al (2010) Hierarchical nanocomposites of polyaniline nanowire arrays on graphene oxide sheets with synergistic effect for energy storage. *ACS Nano* 4:5019–5026. <https://doi.org/10.1021/nn1006539>
85. Mooss VA, Athawale AA (2016) Polyaniline–graphene oxide nanocomposites: Influence of nonconducting graphene oxide on the conductivity and oxidation-reduction mechanism of polyaniline. *J Polym Sci A Polym Chem* 54:3778–3786. <https://doi.org/10.1002/pola.28277>
86. Economou A, Fielden PR, Packham AJ (1994) Batch and flow determination of uranium (VI) by adsorptive stripping voltammetry on mercury-film electrodes. *Analyst* 119:279. <https://doi.org/10.1039/an9941900279>
87. El-Maali NA, El-Hady DA (1999) Square-wave stripping voltammetry of uranium(VI) at the glassy carbon electrode. Application to some industrial samples. *Electroanalysis* 11:201–206
88. Jnr MH, Spiff AI, Abia A (2004) Studies on the influence of mercaptoacetic acid (MAA) modification of cassava (*Manihot sculenta* Cranz) waste biomass on the adsorption of Cu²⁺ and Cd²⁺ from aqueous solution. *Bull Korean Chem Soc* 25:969–976. <https://doi.org/10.5012/bkcs.2004.25.7.969>
89. Kumar PS, Ramakrishnan K, Kirupha SD, Sivanesan S (2010) Thermodynamic and kinetic studies of cadmium adsorption from aqueous solution onto rice husk. *Braz J Chem Eng* 27:347–355. <https://doi.org/10.1590/S0104-66322010000200013>
90. Duncan DM, Cockayne JS (2001) Application of calixarene ionophores in PVC based ISEs for uranium detection. *Sens Actuators B Chem* 73:228–235. [https://doi.org/10.1016/S0925-4005\(00\)00693-6](https://doi.org/10.1016/S0925-4005(00)00693-6)
91. Gupta VK, Mangla R, Khurana U, Kumar P (1999) Determination of uranyl ions using poly(vinyl chloride) based 4-tert-butylcalix[6]arene membrane sensor. *Electroanalysis* 11:573–576. [https://doi.org/10.1002/\(SICI\)1521-4109\(199906\)11:8%3c573::AID-ELAN573%3e3.0.CO;2-Z](https://doi.org/10.1002/(SICI)1521-4109(199906)11:8%3c573::AID-ELAN573%3e3.0.CO;2-Z)
92. de Ramírez F, M, Varbanov S, Bünzli J-CG, et al (2012) Uranyl complexes formed with a *para-t*-butylcalix[4]arene bearing phosphinoyl pendant arms on the lower rim. Solid and solution studies. *Radiochim Acta* 100:359–369. <https://doi.org/10.1524/ract.2012.1925>
93. Ziółkowski R, Górski Ł, Malinowska E (2017) Carboxylated graphene as a sensing material for electrochemical uranyl ion detection. *Sens Actuators B Chem* 238:540–547. <https://doi.org/10.1016/j.snb.2016.07.119>
94. Guo W, Xu H, Cao X et al (2020) A novel electrochemical determination platform of uranyl ion based on silver nanodendrites-reduced graphene oxide. *Microchem J* 158:105134. <https://doi.org/10.1016/j.microc.2020.105134>
95. Kaur G, Kaur H, Mittal SK (2022) Electrochemical sensor based on ion-selective membrane of silica/polyaniline nano-composites for selective determination of uranyl ions. *Talanta Open* 6:100158. <https://doi.org/10.1016/j.talo.2022.100158>
96. Li Y, Wang Z, Liu C et al (2021) Graphene oxide modified H₄L-ion imprinting electrochemical sensor for the detection of uranyl ions. *Z Anorg Allg Chem* 647:1914–1920. <https://doi.org/10.1002/zaac.202100182>
97. Hansen T, Židek K, Zheng K et al (2014) Orbital topology controlling charge injection in quantum-dot-sensitized solar cells. *J Phys Chem Lett* 5:1157–1162. <https://doi.org/10.1021/jz5001193>
98. Wang H, McNellis ER, Kinge S et al (2013) Tuning electron transfer rates through molecular bridges in quantum dot sensitized oxides. *Nano Lett* 13:5311–5315. <https://doi.org/10.1021/nl402820v>
99. Yu D, Liptak RW, Aggarwal G et al (2013) Tunneling conduction in dense silicon quantum dot/poly (methyl methacrylate) composites. *Thin Solid Films* 527:261–266. <https://doi.org/10.1016/j.tsf.2012.11.056>

100. Porter VJ, Geyer S, Halpert JE et al (2008) Photoconduction in annealed and chemically treated CdSe/ZnS inorganic nanocrystal films. *J Phys Chem C* 112:2308–2316. <https://doi.org/10.1021/jp710173q>
101. Konopka SJ, Bruce M (1970) Diffusion coefficients of ferri- and ferrocyanide ions in aqueous media, using twin-electrode thin-layer electrochemistry. *Anal Chem* 42:1741–1746. <https://doi.org/10.1021/ac50160a042>

Springer Nature or its licensor (e.g. a society or other partner) holds exclusive rights to this article under a publishing agreement with the author(s) or other rightsholder(s); author self-archiving of the accepted manuscript version of this article is solely governed by the terms of such publishing agreement and applicable law.

Publisher's Note Springer Nature remains neutral with regard to jurisdictional claims in published maps and institutional affiliations.